Transactions **of the SMiRT 27**
Yokohama, Japan, March 3-8, 2024
Division IX *(include assigned division number from I to XII and remove this blue explanation text)*

MULTI-MATERIALS COMPONENTS DEVELOPMENT FOR POWER APPLICATIONS BY DIRECTED ENERGY DEPOSITION

Jan DZUGAN[1], Ying LI[2], Daniel MELZER[2], Michal BRAZDA[2], Anna REIS[3], Martina KOUKOLIKOVA[2] and Libor KRAUS[2]

[1] Professor, COMTES FHT, Dobrany, Czech Republic (jan.dzugan@comtesfht.cz)
[2] Research Scientist, COMTES FHT, Prumyslova 995, Dobrany, Czech Republic
[3] Research Scientist, Inegi, Campus da FEUP, Rua Dr. Roberto Frias, 400 4200 - 465 Porto, Portugal

ABSTRACT

In many industrial applications, single-material components struggle to meet all operational demands, necessitating the development of multi-material components. The need to join dissimilar materials, a task preferably managed in controlled factory conditions rather than during on-site assembly, is a significant factor driving this trend. Using components that transition between materials ensures similar-material welds during final installation, simplifying and securing the assembly process. This paper explores key factors influencing the joint quality of multi-material components, focusing on connections between Inconel alloys 718 and 625 with austenitic 316L stainless steel and martensitic 42C stainless steel. All materials are applied using powder-blown laser directed energy deposition methods. The study highlights the importance of deposition sequence for the material pairs Inconel 718 – SS316 and Inconel 625 – SS42C, and examines how interface orientation and surface quality influences the joint quality in the former pair.

INTRODUCTION

In the innovative field of additive manufacturing (AM), specifically with directed energy deposition (DED) methods, there has been a significant advancement in the generation of functionally graded materials (FGMs). These materials are increasingly used in a variety of sectors, including but not limited to, the production of engine components, healthcare devices, components of turbines, railway system maintenance, and aerospace engineering (Lai *et al.*, 2017; Guo *et al.*, 2019; Liu *et al.*, 2020; Panchal and K, 2022). The sophisticated features of AM, such as producing intricate designs, the ability to tailor to specific needs, and the precise control of material properties within individual parts, are well-recognized in the body of research emerging in recent times (Additive Manufacturing Research Group, 2018; Saleh *et al.*, 2020; ISO/ASTM, 2022).

Earlier studies in this domain primarily concentrated on exploring the attributes of AM with single materials (Rzepa *et al.*, 2021, 2023; Urbánek *et al.*, 2022). Present research trends, however, are pivoting towards FGMs, with a special emphasis on those created using powder bed fusion (PBF) or DED methods (Bandyopadhyay, Zhang and Onuike, 2022). The powder blown laser DED approach is particularly distinguished for its efficacy in layering multi-material systems, owing to its unique powder feeders and adaptable processing parameters for each successive layer. The utility of DED in repairing components, accommodating the use of varying material types or batches, underscores its capacity to manage diverse materials effectively (Dass and Moridi, 2019; Saboori *et al.*, 2019; Sing *et al.*, 2019).

Recently, there has been a notable focus on FGMs that are characterized by chemical composition variations, especially the integration of different grades of Fe-based stainless steel with Ni-based Inconel alloys. This is evident in the frequent use of combinations like Inconel 625 and Inconel 718 with SS316L or SS304 in scholarly articles over the past decade (Savitha *et al.*, 2015; Carroll *et al.*, 2016; Konečná *et al.*, 2016; Koike *et al.*, 2019; Chen *et al.*, 2020; Feenstra, Molotnikov and Birbilis, 2020; Yang *et al.*, 2022). The compatibility and combined attributes of these materials have been advantageous. However, the overall structural strength and mechanical characteristics of the resulting materials are intricately linked to the selected process parameters and the approach to construction. Factors such as the order of material layering, the orientation of interfaces, and the quality of surfaces play a crucial role, as elaborated in recent studies (Melzer *et al.*, 2021a, 2022; Halmešová *et al.*, 2022; Koukolíková *et al.*, 2022; Melzer, Gil, *et al.*, 2023; Melzer, Koukolíková, *et al.*, 2023). This study focuses on elucidating the influence of these vital elements on the structural and mechanical integrity of the materials.

Materials and method

The components investigated here were deposited by powder blown laser directed energy deposition (L-DED) systems. The materials combination of Inconel 718 and stainless steel 316 were deposited by INSSTEK MX 600 equipped with 2 kW Yttrium fibre laser. While the combinations of Inconel 625 and martensitic stainless steel 42C were deposited by machine consisting of a modular coaxial processing head and equipped with a fibre-coupled laser diode, model Laserline LDF 3000–100, with a nominal beam power of 6000 W. The powder nozzle is mounted on a KUKA KR 90 R3100 industrial robot, with six axes connected to the robot control unit. More details about the experiments can be found in the previous studies (Melzer *et al.*, 2021a, 2022; Melzer, Gil, *et al.*, 2023; Melzer, Koukolíková, *et al.*, 2023).

Results and discussion

The specimens obtained are depicted in Figure 1. For the materials combination of IN718 and SS316L, various deposition angles for material interfaces, ranging from horizontal to vertical directions, were explored (Figure. 1a-d). For samples with inclined planes, there were two variants: one with a machined surface on the first deposited material before adding the second materials (Figure 1c), and the other with the as-deposited interface between the materials (Figure 1d). In the combination of IN625 and 42C steel, horizontal deposition with varying sequences of material deposition was employed. Metallographic as well as mechanical properties investigations were carried out.

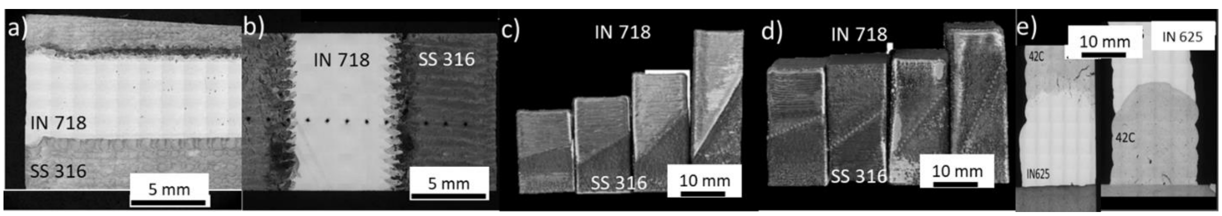

Figure 1 Deposited multi-material combinations: a) Vertical interface IN 718-SS316 [1, 2], b) horizontal interface IN 718-SS316 [3], c) Inclined machined interface IN 718-SS316 [4], c) Inclined as-deposited interface IN 718-SS316 [4], e) Horizontal interface IN 625-42C

Figure 2 shows the microstructure characterization of the YZ plane of the horizontals blocks with varying deposition order in the SS316L/IN718 material. Optical micrographs in Figure 2(a) and (c) reveal two distinct interface types formed by altering the deposition order in the IN718 and SS316L system. When IN718 was deposited onto previously deposited SS316L, it created a sharp interface (H-type I), characterized by a clear, flat borderline where the material type changed rapidly, as shown in Figure 2(a). conversely, when SS316L was subsequently deposited on the IN718 layer (H-type II), a more gradual interface with distinct material mixing in the melt pools was observed, as depicted in Figure 2(c). Both types achieved a low porosity level of 0.011%, with over 90% of observed globular pores having a diameter below 20 μm. EBSD in Figures 2(b) and (d) provided further insights into the differences near each transition type. In the case of H-type I, a sharp transition from 316L to IN718 was accompanied by a change in chemical composition, but a continuation of grain growth with the same crystallographic orientation across the interface was observed. As grain growth progressed, the fine-grained microstructure of 316L transformed into the coarse-grained columnar structure of IN718, with the columnar grains of IN718 growing perpendicular to the interface. In the case of H-type II, where material mixing occurred, no crystallographic traceability of grains was observed, although some exceptions were noted. Interestingly, grains on the 316L side exhibited the same coarseness as IN718.

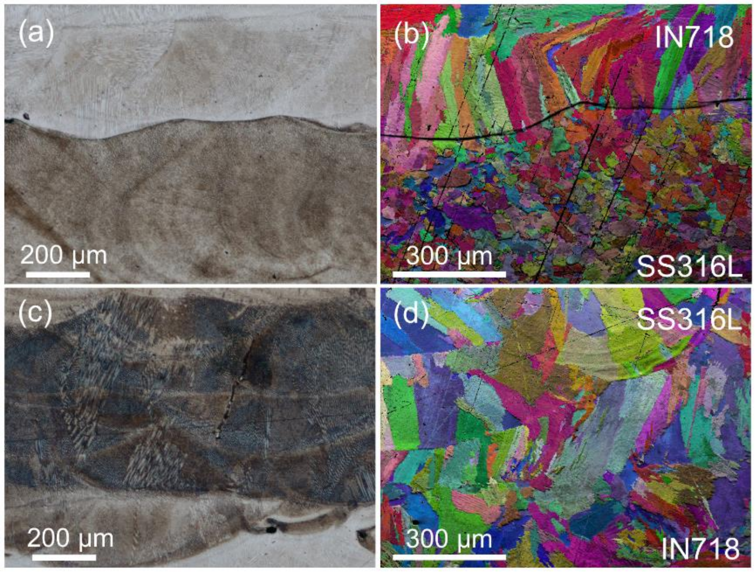

Figure 2 Optical micrographs (a) H-type I (c) H-type II; EBSD-IPF (b) H-type I (d) H-type II.

The effect of deposition sequence on the microstructure in the IN625/42C material system was also investigated, as illustrated in Figure 3. Notable disparities in structural integrity were evident when comparing H-joint I (where 42C was deposited on IN625) with H-joint II (IN625 deposited on 42C). Each joint exhibited a distinct propensity for defect formation, with IN625 showing fewer defects and 42C presenting more. Notably, the nature of the interface created varied considerably with the deposition order. In H-joint I, defects tended to spread more into the IN625 region (Figure 3(a)), whereas H-joint II displayed a reduced incidence of cracks in the 42C area, and the adjacent IN625 zone remained largely defect-free (Figure 3(b)). Porosity at the interfaces measured approximately 1.91% for H-joint I and significantly less, at 0.14%, for H-joint II. There was also a marked difference in the joint geometry; the fusion line of H-joint II notably dipped downwards, resulting in a joint height disparity of 1000 µm for H-joint II compared to 700 µm for Joint I.

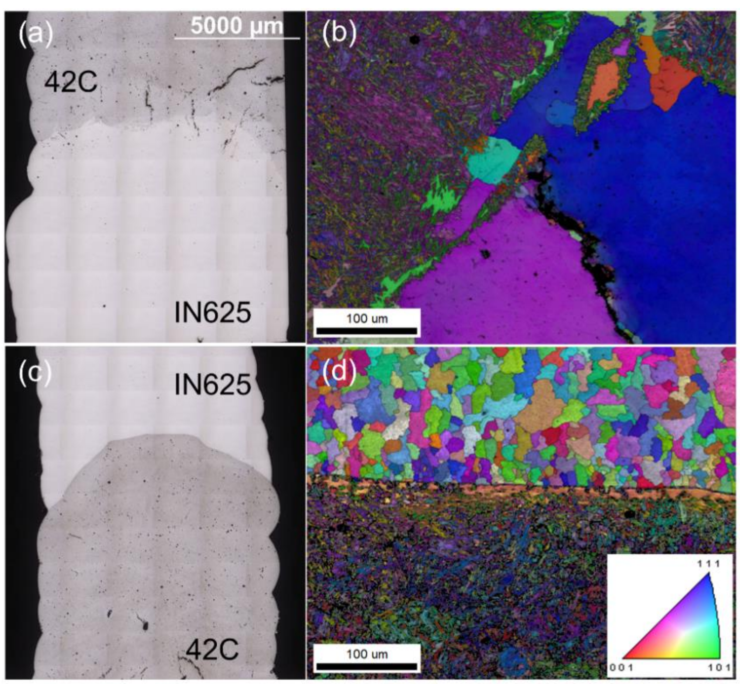

Figure 3 Optical micrographs (a) H-joint I (c) H-joint II; EBSD-IPF (b) H-joint I (d) H-joint II.

The Electron Backscatter Diffraction (EBSD) analysis, as shown in Figure 3(b) and (d), provides further insight into the grain structure, phase, and orientation near the interfaces of both joints. The IN625 zone exhibited a Face-Centered Cubic (FCC) structure, while the 42C zone was identified with a Body-Centered Cubic (BCC) structure. In Joint I, the interface between IN625 and 42C did not show a sharp demarcation. Instead, there was a gradual compositional transition, allowing for isolated BCC phase (42C) segments to be surrounded by the FCC phase (IN625), as seen in Figure 3(b). Additionally, intergranular cracks were more prevalent on the 42C side of Joint I. These cracks, formed during the solidification at the interface, could be attributed to the segregation of certain alloying elements along the grain boundaries due to uneven solidification. In contrast, Joint II exhibited a stark contrast at the interface, with a sharp division between the bottom BCC phase (42C) and the upper FCC phase (IN625), as depicted in Figure 3(d). Here, a coarse-grained band separated the fine-grained 42C zone from the coarse-grained IN625 area. Energy Dispersive Spectroscopy (EDS) analysis revealed this band as part of the 42C. The grain enlargement in this region might result from the additional heat during IN625 deposition. The pronounced fusion line in Joint II suggested minimal mixing of materials within the melt pool, though diffusion of main elements like Fe and Ni could be anticipated based on other studies on bimetallic joints (Melzer *et al.*, 2022). In Joint II, the IN625 side showed no defects, in contrast to the 42C side, where cracks and other defects were predominantly observed.

The impact of varying deposition orders on mechanical properties was assessed in both SS316L/IN718 and IN625/42C material systems. Figure 4 presents the tensile properties at room temperature for all conditions under investigation. It was observed that in the SS316L-IN718 system, the sharp interface (type I) consistently demonstrated superior tensile characteristics compared to the gradual interface (type II). Notably, the tensile results for the gradual interface showed a higher degree of variability, which could be attributed to the non-uniform distribution of defects within these interfaces. Interestingly, despite the lower ultimate tensile strength (UTS) and elongation values in the gradual interface, similar offset yield strength (OYS) levels were observed across several specimens. This phenomenon, where the elastic portions of the stress-strain curves remained unchanged, suggests that the differences in mechanical properties might be rooted in the varying densities of structural defects. Further insights into this aspect are discussed in our previous study (Melzer *et al.*, 2021a).

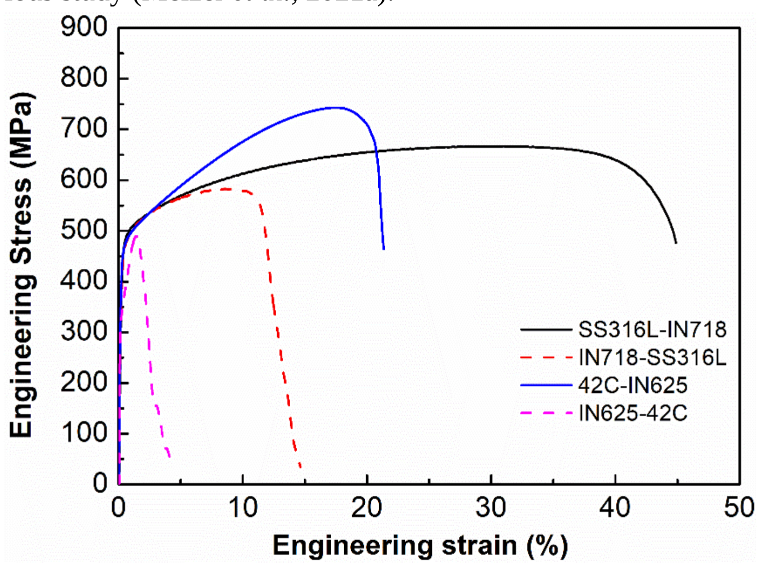

Figure 4 Mechanical properties of material system SS316L/IN718 and IN625-42C with various deposition sequence.

In the context of IN625/42C joints, the tensile results for the Joint I sample indicated a reduction in OYS, UTS, and ductility when compared to the Joint II sample. This diminished strength and ductility in Joint I could be attributed to premature failure during testing, highlighting the impact of microstructural integrity on mechanical performance. The tensile tests for Joint I revealed that the juxtaposition of a crack-free structure (IN625) on one side and a fractured structure (42C) on the other was detrimental to tensile behavior. Defects near the interface likely served as stress concentrators, predisposing the location of failure and diminishing the overall mechanical performance. These findings align with microstructural examinations that uncovered a significant presence of manufacturing-induced cracks. Nevertheless, to comprehensively assess the strength and integrity of the bimetallic joint, it is essential to pinpoint the exact location of specimen failure, thereby determining if the joint's performance surpasses that of the individual materials. Additional details and analysis are available in the earlier study (Melzer, Gil, *et al.*, 2023).

The impact of interface orientation between dissimilar materials during the deposition process is a crucial determinant of joint quality. An investigation into this factor involved manufacturing continuous blocks with interface angles of 15°, 30°, 45°, and 60°. Micrographic analysis reveals a direct relationship between interface angle and porosity level and distribution. At a 15° angle, pores are uniformly distributed throughout the material volume. However, at angles of 30° and 45°, not only are larger defects concentrated within the interface zone, but their density also increases. The situation is further exacerbated at a 60° angle, where the average pore size is even larger. Figure 5 shows the measured porosity increases with the interface angle in various zones, including single-material areas of SS316L and IN718 and the interface zone between them. Interestingly, porosity in the individual materials does not vary with interface angle changes, but porosity near the interface region does, particularly showing a marked increase at 60°.

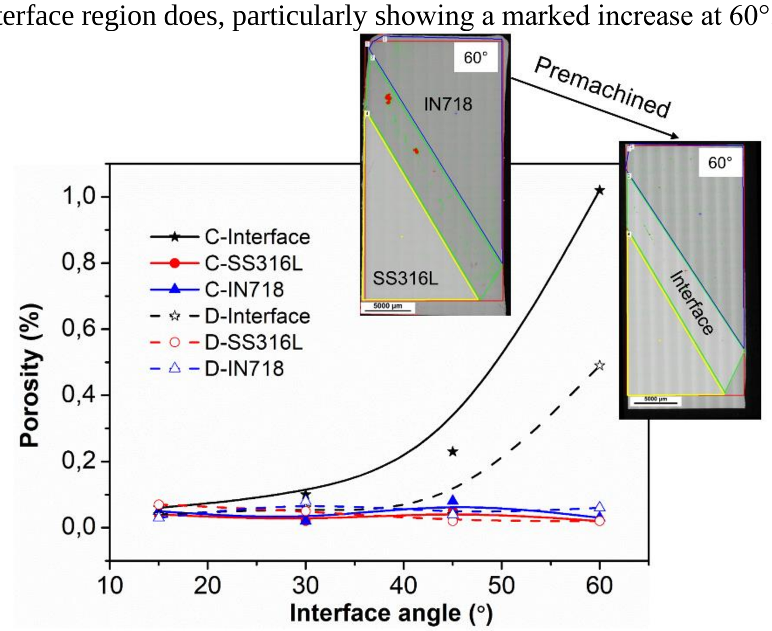

Figure 5 Porosity evolution with increasing of interface orientation of various measured zones in SS316L/IN718 material system.

To evaluate the effect of surface quality on the joining of dissimilar materials, blocks with various interface orientations were initially deposited (SS316L), machined, and then used as substrates for depositing the second material (IN718). These pre-machined blocks, labeled as D-, contrast with the continuous blocks, C-. It was observed that, compared to the C-blocks, the increase in pore size and concentration at the interface was less pronounced for interfaces inclined at 15°, 30°, and 45°, with the most significant reduction occurring at 60°. Despite a higher number of pores at this angle, the decrease in porosity at 60° is clearly demonstrated in Figure 5. Furthermore, the porosity levels for both single materials did not exceed 0.08%, regardless of their continuous or pre-machined state. However, at the interface, the continuous deposition strategy resulted in a significant increase in porosity, more than doubling that of the pre-machined block for a 60° angle. This interface appearance at 60° closely resembles a near-vertical orientation from previous studies (Melzer *et al.*, 2022). Pre-machining the surface can effectively remove detrimental features commonly found post-DED process, such as unmelted particles, surface roughness variations, porosity, and surface defects, thereby contributing positively to the formation of high-quality joints. Additionally, continuous blocks maintained a porosity level below 0.08% up to a 45° angle. However, for continuous blocks, the porosity rapidly increased with the interface angle, particularly from 30° to 60°, where it exceeded 1%. At lower angles, the pre-machining process, implemented before the deposition of IN718, proved effective in reducing the formation of defects by cleaning the surface of unmelted particles and enhancing material fusion. However, this benefit diminishes beyond a 60° threshold, where the change in surface tension and melt pool stability leads to defect formation. When material is deposited at a steeper interface angle, surface tension forces can cause the material to form irregular shapes, promoting the development of pores and voids. In summary, an inclined substrate can destabilize the melt pool of the deposited material, affecting material flow and stability.

Figure 6 displays characteristic tensile curves for both C- and D- blocks with varying interface angles. Figure 7 offers a comprehensive view of the tensile property trends across the manufactured blocks. Previous result of horizontal (C0) and vertical block (C90) were also added here for comparison (Melzer *et al.*, 2021b, 2022). Starting from the lower interface angles on the graph, it becomes clear that even a minor 15° angle in a continuous interface can significantly reduce strength and elongation when compared to a conventional horizontal interface orientation. Notably, the OYS, ranging from 396 to 464 MPa, and UTS, between 519 to 562 MPa, show minimal sensitivity to changes in interface angle from 15 to 60° in continuous blocks. Conversely, elongation decreases markedly across this range of angles, with a drastic 80% drop observed at the 60° interface. A notable 70% reduction in elongation is already evident at the 30° interface angle. For vertical interfaces (Melzer *et al.*, 2022), the results are markedly lower, with a pronounced decrease in strength.

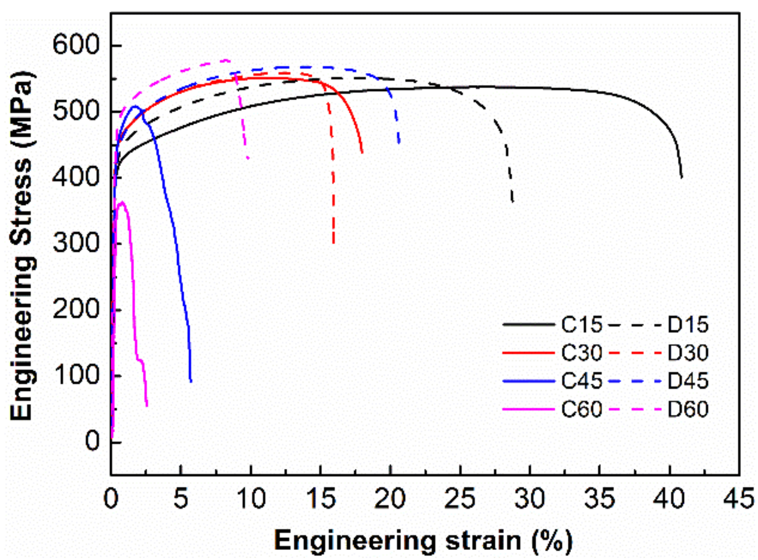

Figure 6 Representative tensile curves of C- and D-sample consisting of two materials.

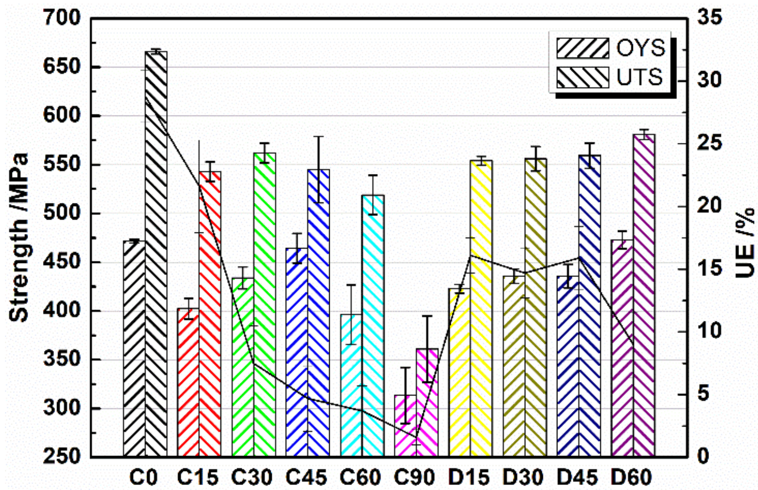

Figure 7 Summary of tensile results of continuous and discontinuous blocks supplemented by results of horizontal and vertical block. Note that data of CO from (Melzer *et al.*, 2021a), and C90 from (Melzer *et al.*, 2022).

The tensile outcomes for discontinuous D-blocks, depicted on the right side of the graph, demonstrate a different pattern. While UTS and OYS values are comparable to those of C-blocks, the variations in OYS and UTS between different angles are less pronounced, ranging from 422 to 473 MPa and 554 to 580 MPa, respectively. Although the elongation values for discontinuous blocks do not match the results for C15, they exhibit greater consistency across 15, 30, and 45° angles, achieving over 50% of the horizontal interface results. The uniform elongation (UE) experiences a significant reduction at the 60° angle; however, the final value is still twice as high as that for the 60° continuous block.

Structural integrity and mechanical properties are observed to degrade with interface angles above 60°. To understand the deposition process for geometries with 90° corners, an extreme condition of a 90° interface angle is examined, as depicted in Figure 8, showing porosity and hardness measurements across SS316L and IN718 zones. Porosity analysis in the YZ plane revealed globular pores regularly distributed, particularly aligned along zones corresponding to different materials. These defects, predominantly oriented at angles between 10° to 35° relative to the deposition direction, resulted in a total porosity of 0.45% in the affected areas. The hardness profile varies regularly with material type. In the SS316L zone, hardness starts at 200 HV5, dropping to 157 HV5 due to defect concentration. In the IN718 area, it increases to an average of 268 HV. A notable drop to 160 HV5 occurs in the transition area between 316L and IN718 due to defects.

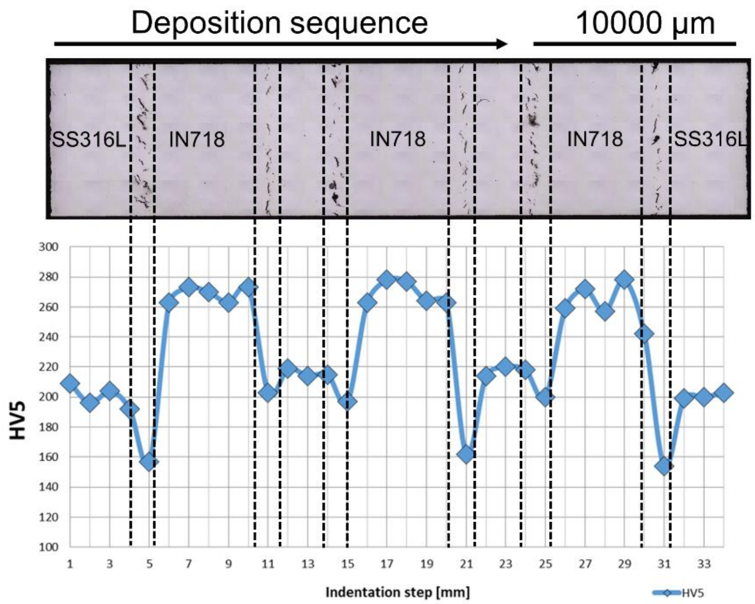

Figure 8 Porosity and hardness measurement profile across the deposited zones of SS316L and IN718.

EBSD analysis was performed on the interface zone including the transition from SS316L to IN718 (V-type I) and vice versa (V-type II), as illustrated in Figure 9. The yellow dotted lines in the images indicate the sharp boundary of base elements distribution. In the V-type I interface, predominantly coarse grains without preferential orientation and elongated in the deposition direction were observed in Figure 9(a). Inter-granular cracks were identified in the 316L area for both interface types. The grain orientation of deposited IN718 largely mirrored the original orientations of 316L grains. Near V-type I interface, IN718 exhibited large, expressively oriented (111) grains along the material boundary in (1) zone, followed by zones of rapidly refined grains in (2) zone. Further from this zone, a mix of coarse and smaller columnar IN718 grains was noted. Conversely, interface V-type II on the IN718 side featured a combination of coarse and fine columnar grain zones in Figure 9(b). At the sharp transition, some SS316L grains matched the crystallographic orientation of adjacent IN718 grains. However, new columnar SS316L grains with different orientations also formed at the interface. Away from the boundary, the 316L side predominantly had coarse grains. Intergranular cracks were noted in the pure SS316L area, as shown in (3) marked in Figure 9(b).

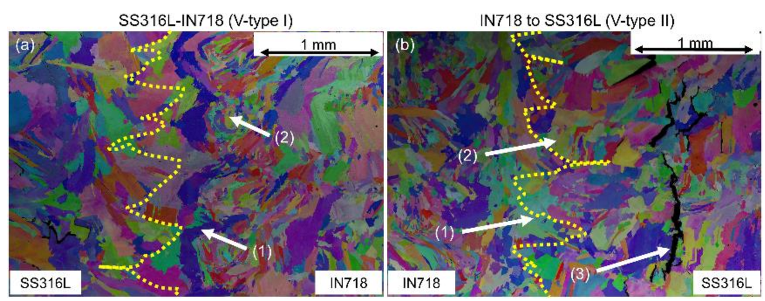

Figure 9 EBSD images of the two interface type, (a) V-type I and (b) V-type II

CONCLUSION

This study highlights the advanced capabilities of AM, particularly DED, in producing FGMs for various applications. The research demonstrates that factors like deposition order, interface orientation, and surface quality significantly influence the structural integrity and mechanical properties of materials, especially in combinations of Fe-based stainless steel and Ni-based Inconel alloys. It was found that better joint quality is consistently achieved when Inconel is applied onto a steel substrate in the material combinations examined. Additionally, the investigation into the impact of inclined surface orientation on joint quality showed more pronounced effects for as-deposited interfaces. The most favourable outcomes were observed with horizontal interface orientations, with a slight decrease in properties for angles up to 45° on machined surfaces and up to 30° for as-deposited interfaces.

REFERENCES

Additive Manufacturing Research Group (2018) *The 7 Categories of Additive Manufacturing, Loughborough University*.
Bandyopadhyay, A., Zhang, Y. and Onuike, B. (2022) ‘Additive manufacturing of bimetallic structures’, *Virtual and Physical Prototyping*. Taylor & Francis, 17(2), pp. 256–294. doi: 10.1080/17452759.2022.2040738.
Carroll, B. E. *et al.* (2016) ‘Functionally graded material of 304L stainless steel and inconel 625 fabricated by directed energy deposition: Characterization and thermodynamic modeling’, *Acta Materialia*. Elsevier Ltd, 108, pp. 46–54. doi: 10.1016/j.actamat.2016.02.019.
Chen, N. *et al.* (2020) ‘Microstructural characteristics and crack formation in additively manufactured bimetal material of 316L stainless steel and Inconel 625’, *Additive Manufacturing*. Elsevier, 32(January), p. 101037. doi: 10.1016/j.addma.2020.101037.
Dass, A. and Moridi, A. (2019) ‘State of the art in directed energy deposition: From additive manufacturing to materials design’, *Coatings*. doi: 10.3390/COATINGS9070418.
Feenstra, D. R., Molotnikov, A. and Birbilis, N. (2020) ‘Effect of energy density on the interface evolution of stainless steel 316L deposited upon INC 625 via directed energy deposition’, *Journal of Materials Science*, 55(27), pp. 13314–13328. doi: 10.1007/s10853-020-04913-y.
Guo, Z. *et al.* (2019) ‘An Al-7Si alloy/cast iron bimetallic composite with super-high shear strength’, *Journal of Materials Research and Technology*. doi: 10.1016/j.jmrt.2017.06.014.
Halmešová, K. *et al.* (2022) ‘Effect of laser power on thermal properties of multimaterial structure Inconel 718 and stainless steel 316L processed by directed energy deposition’, *Journal of Alloys and Compounds*. Elsevier, 927, p. 167082. doi: 10.1016/j.jallcom.2022.167082.
ISO/ASTM (2022) ‘ISO/ASTM 52909: Additive manufacturing of metals — Finished part properties — Orientation and location dependence of mechanical properties for metal powder bed fusion’, *International Standard*.
Koike, R. *et al.* (2019) ‘Graded inconel 625 - SUS316L joint fabricated using directed energy deposition’, *International Journal of Automation Technology*. doi: 10.20965/ijat.2019.p0338.
Konečná, R. *et al.* (2016) ‘Fatigue crack growth behavior of Inconel 718 produced by selective laser melting’, *Frattura ed Integrita Strutturale*. doi: 10.3221/igf-esis.35.04.
Koukolíková, M. *et al.* (2022) ‘The influence of laser power on the interfaces of functionally graded materials fabricated by powder-based directed energy deposition’, *Journal of Materials Science*, 57(28), pp. 13695–13723. doi: 10.1007/s10853-022-07453-9.
Lai, Q. *et al.* (2017) ‘Investigation of a novel functionally graded material for the repair of premium hypereutectoid rails using laser cladding technology’, *Composites Part B: Engineering*. doi: 10.1016/j.compositesb.2017.07.089.
Liu, Z. *et al.* (2020) ‘Laser additive manufacturing of bimetallic structure from Ti-6Al-4V to Ti-48Al-2Cr-2Nb via vanadium interlayer’, *Materials Letters*. doi: 10.1016/j.matlet.2019.127210.
Melzer, D. *et al.* (2021a) ‘Structural integrity and mechanical properties of the functionally graded material based on 316L/IN718 processed by DED technology’, *Materials Science and Engineering: A*, 811(March). doi: 10.1016/j.msea.2021.141038.
Melzer, D. *et al.* (2021b) ‘Structural integrity and mechanical properties of the functionally graded material based on 316L/IN718 processed by DED technology’, *Materials Science and Engineering A*, 811(August 2020), p. 141038. doi: 10.1016/j.msea.2021.141038.

Melzer, D. *et al.* (2022) 'Fracture characterisation of vertically build functionally graded 316L stainless steel with Inconel 718 deposited by directed energy deposition process', *Virtual and Physical Prototyping*, 17(4), pp. 821–840. doi: 10.1080/17452759.2022.2073793.
Melzer, D., Gil, J., *et al.* (2023) 'Ambient and high temperature tensile behaviour of DLD-manufactured inconel 625/42C steel joint', *Materials Science and Engineering: A*, 885(June). doi: 10.1016/j.msea.2023.145603.
Melzer, D., Koukolíková, M., *et al.* (2023) 'Influence of interface orientation and surface quality on structural and mechanical properties of SS316L/IN718 block produced using directed energy deposition', *Surfaces and Interfaces*, 41(February). doi: 10.1016/j.surfin.2023.103139.
Panchal, Y. and K, P. (2022) 'Functionally graded materials: A review of computational materials science algorithms, production techniques, and their biomedical applications', *Proceedings of the Institution of Mechanical Engineers, Part C: Journal of Mechanical Engineering Science*. doi: 10.1177/09544062221109261.
Rzepa, S. *et al.* (2021) 'Tensile properties evaluation of additively manufactured AISI 316L thin wall and bulk material using various miniaturized specimen geometries', *IOP Conference Series: Materials Science and Engineering*. doi: 10.1088/1757-899x/1178/1/012048.
Rzepa, S. *et al.* (2023) 'Effect of ECAP processing on microstructure and mechanical behaviour of Ti-6Al-4V manufactured by directed energy deposition', *Materials Characterization*, 196, p. 112622. doi: https://doi.org/10.1016/j.matchar.2022.112622.
Saboori, A. *et al.* (2019) 'Application of directed energy deposition-based additive manufacturing in repair', *Applied Sciences (Switzerland)*, 9(16). doi: 10.3390/app9163316.
Saleh, B. *et al.* (2020) '30 Years of functionally graded materials: An overview of manufacturing methods, Applications and Future Challenges', *Composites Part B: Engineering*. Elsevier Ltd, 201(August), p. 108376. doi: 10.1016/j.compositesb.2020.108376.
Savitha, U. *et al.* (2015) 'Chemical analysis, structure and mechanical properties of discrete and compositionally graded SS316-IN625 dual materials', *Materials Science and Engineering A*. doi: 10.1016/j.msea.2015.09.001.
Sing, S. L. *et al.* (2019) '3D printing of metals in rapid prototyping of biomaterials: Techniques in additive manufacturing', in *Rapid Prototyping of Biomaterials: Techniques in Additive Manufacturing*. doi: 10.1016/B978-0-08-102663-2.00002-2.
Urbánek, M. *et al.* (2022) 'Prediction of Behaviour of Thin-Walled DED-Processed Structure: Experimental-Numerical Approach', *Materials*. doi: 10.3390/ma15030806.
Yang, S. W. *et al.* (2022) 'Defect of functionally graded material of inconel 718 and STS 316L fabricated by directed energy deposition and its effect on mechanical properties', *Journal of Materials Research and Technology*. The Authors, 17, pp. 478–497. doi: 10.1016/j.jmrt.2022.01.029.